Title:	Non-Linearity correction procedures studies for the NISP instrument
Reference:	
Issue:	1.3
Date:	31/10/2012
Custodian:	

Authors:		Date:	Signature:
A. Chapon J.C. Clemens A. Ealet F. Marmol A. Secroun G. Smadja			
Approved:		Date:	Signature:
Authorized:		Date:	Signature:

Contents

1 Introduction and goal

The NISP instrument aboard Euclid will host 16 HgCdTe detectors of 2048×2048 hybrid pixels. If their response could be expected to be linear over a small range of fluxes, it will not be the case of Euclid science. Non-linearity is a fundamental parameter of detectors that must be and can be corrected for. It may be seen as a change in the rate that charge is accumulated under constant source flux as a function of the amount of charge already stored. The purpose of this document is to define and optimize calibration strategies regarding the correction of non-linearity effect for these detectors and compare strategies that could be applied in-flight to those on-ground.

Euclid science requires non-linearity correction to be performed to an accuracy of 0.3% for photometry and 1.5% for spectroscopy. This correction is strongly dependent on the read mode and the integrated flux. The baseline plans different read modes for photometry and spectroscopy that must be considered here: 100s integration time Fowler-16[1] read mode for photometry and 560s integration time multi-4×37[2] for spectroscopy.[?] Also, most observed galaxies will present a maximal flux of 1 to 2 electrons per pixel and per second on the detector, while only a few galaxies and stars will cause the saturation of the detector ($\sim$100 e$^-$/pix/s). Therefore, since not specified, previous requirements are supposed to be applicable to integrated fluxes of 1000 electrons per pixel.

As an ideal detector is supposed to be linear in its response, non-linearity may be derived as the deviation from the best fitting line to the low-signal portion of the data in an illuminated exposure. Precisely, the high flux portion must clearly be excluded since saturation causes a strong departure from the linear fit. As for the very low portion, the deviation from linear fit due to reset anomaly is not considered here, but possible reset anomaly and reciprocity failure are discussed in section 7.

Non-linearity correction is based on a polynomial of degree 4 for which four coefficients may be derived for each pixel individually. We have studied two possible strategies for the correction of the non-linearity effect:
- *in-flight correction*: it consists in correcting each read by the same correction function (namely the same four coefficients) for all the pixels. That is due to the fact that in-flight processing does not enable to store individual pixel coefficient maps.
- *on-ground correction*: the correction can be tuned for each pixel of the detector but applied only on the final straight line (in-flight linear fit), because frames can not be sent on-ground due to bandwidth limitations.

In the following, section 2 describes JWST data on which both strategies have been tested. Section 3 shows how pixel values are simulated from JWST data and how non-linearity correction is applied both with in-flight and on-ground methods. The following sections give the systematic errors induced by each method and evaluate the accuracy achieved by each method for Euclid science read modes varying fluxes and the number of calibration exposures. Finally, in section 7, some experimental tests are proposed to evaluate the necessity of taking reset anomaly and reciprocity failure into account for Euclid's detectors.

---

[1]Fowler-16 means 2 groups of 16 frames averaged together, one group at the start and one at the end of the 100s.

[2]multi-4×37 means 37 groups of 4 frames averaged together, acquired in non-destructive reads, the groups being regularly spaced over the 560s.

2 Study of JWST "real" data

JWST data have been acquired on-ground on an H2RG detector similar to that foreseen for Euclid: same number of pixels but slightly longer cutoff (2.5 μm). The obtained non-linearity effect of JWST data is shown in figure 1 and appears in blue. The linear ideal signal is shown in red for comparison.

Figure 1: Non-linearity effect for JWST data in ADU count
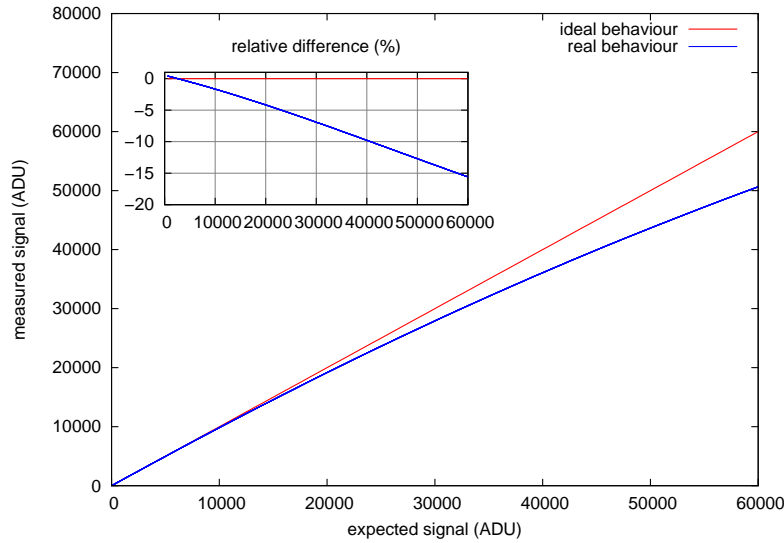
Non-linearity correction coefficients are available for individual pixels. They have been derived from the assumption that the true signal S of each pixel can be fitted by a polynomial of degree four to the measured signal ADU_i such that:[3]

$$S(ADU_i) = g_i \times (a_1(i) \times ADU_i + a_2(i) \times ADU_i^2 + a_3(i) \times ADU_i^3 + a_4(i) \times ADU_i^4)$$

In this model, a_1, a_2, a_3 and a_4 are the non-linearity correction coefficients of JWST data. This equation should be read as S evolves linearly with time, while ADU_i does not. For the purpose of this study, the gains g_i of all pixels are assumed to be taken equal to one.

Figure 2 presents the maps of the four non-linearity correction coefficients obtained by the JWST team on one of their detectors. As may be seen in the figure, the values of the correction coefficients are not uniform and a similar pattern seems to appear in all maps.

Coefficients $\{a_1, a_2, a_3, a_4\}$ can also be plotted as histograms as shown in figure 3. These histograms are consistent with gaussian distributions. The mean values and standard deviations thus derived are summarized in table 1.

Considering the pattern that appears in figure 2, it is relevant to check for correlations between coefficients. That is the purpose of figure 4. As may be seen in this figure, it is important to note that a_2, a_3, a_4 are not strongly correlated to a_1, but are actually correlated with each other.

---

[3]Subscript i refers to one pixel of the H2RG 2048x2048 detector.

Figure 2: From left to right: a_1, a_2, a_3, a_4 coefficients maps from JWST data
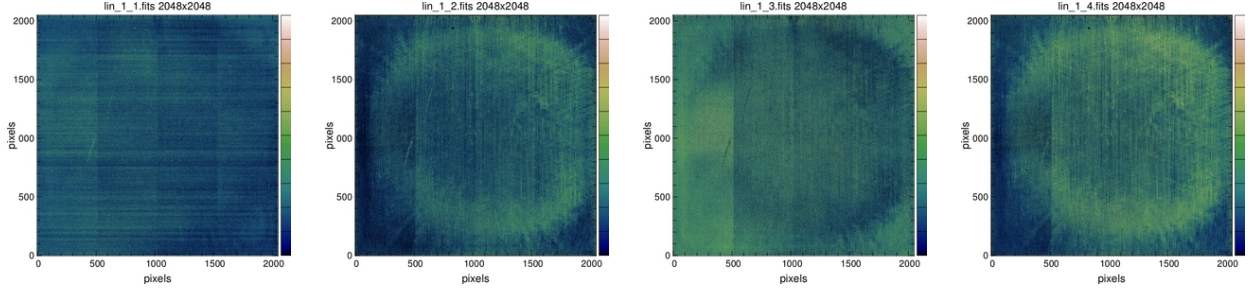

Figure 3: Dispersion of the $\{a_1, a_2, a_3, a_4\}$ JWST correction coefficients and gaussian fit (blue line)
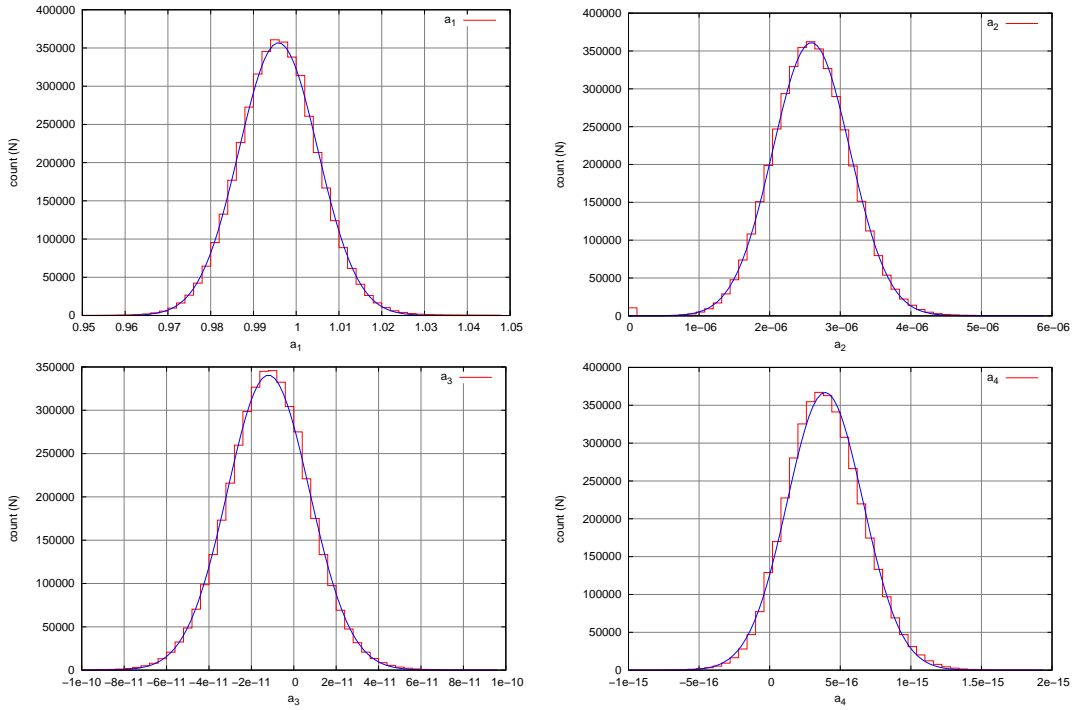

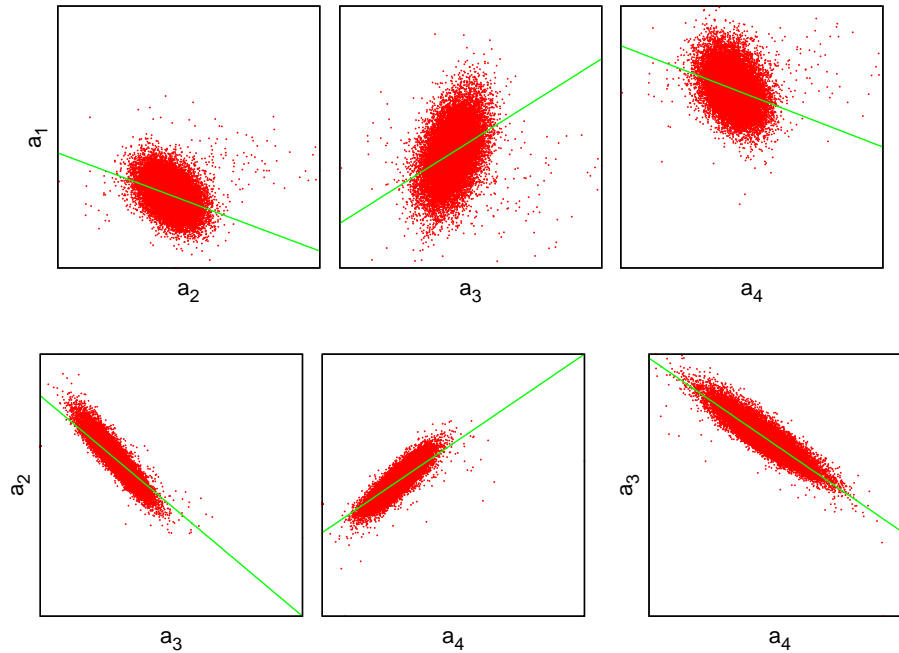Table 1: Mean values and standard deviations of $\{a_1, a_2, a_3, a_4\}$ JWST correction coefficients

| Correction coefficient	mean value $\langle a_j \rangle$	standard deviation σ_j
a_1	0.99984	0.010499
a_2	$2.5888\mathrm{e}^{-6}$	$5.7757\mathrm{e}^{-6}$
a_3	$-1.1896\mathrm{e}^{-11}$	$1.9528\mathrm{e}^{-11}$
a_4	$3.9333\mathrm{e}^{-16}$	$2.7397\mathrm{e}^{-16}$

Figure 4: Correlations of coefficients

3 Simulation of data and non-linearity correction methods

3.1 Simulation of pixel response

Hereafter is described one way to simulate the response of a pixel. For each simulated pixel, an ideal signal is generated without any read noise. As the incoming flux is constant, this signal is expected to increase linearly with time. However, as the detector is non-linear, a non-linearity effect has to be applied to each read to reconstruct the simulated "actual" response of the pixel. Figure 5 shows the construction of the non-linear response (red line) from the ideal linear response (green line).

Figure 5: Simulation of a pixel response: a non-linear effect is applied to the expected (ideal) signal.
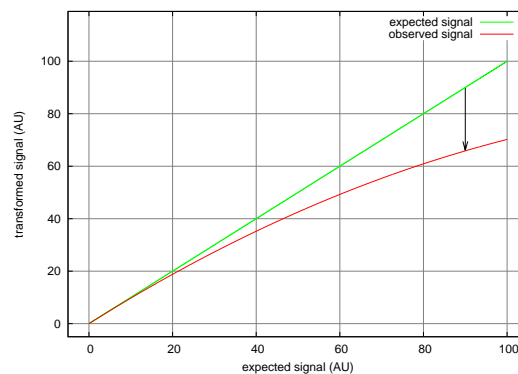
As non-linearity correction depends on the correction method used and on the accuracy on the

$\{a_1, a_2, a_3, a_4\}$ coefficients, the non-linear effect applied here is based on the draw of new coefficients attributed to the simulated pixel and its application is then obtained from the inverse transformation $u_i(ADU)$ (which is the non-linearity effect) verifying for each pixel i:

$$(a_1(i) \times ADU + a_2(i) \times ADU^2 + a_3(i) \times ADU^3 + a_4(i) \times ADU^4)$$
$$\times u_i(ADU) \quad = \quad 1$$

The inverse transformation $u_i(ADU)$ has been calculated thanks to the Newton-Raphson method. The simulation is constructed from the draw of 10000 pixels from JWST data and has been chosen so as to satisfy properties that have been observed on JWST data (as seen in section 2):
  – the correlation of the non-linearity correction coefficients $\{a_1, a_2, a_3, a_4\}$;
  – their Gaussian distributions ;
  – their spatial dispersion over the pixels of the detector, as expressed by the standard deviations $\{\sigma_1, \sigma_2, \sigma_3, \sigma_4\}$.
In order to take into account the possible influence of these properties, coefficients (denoted $\{a_1^\delta, a_2^\delta, a_3^\delta, a_4^\delta\}$) attributed to the simulated pixel have been defined from a "double" draw. Precisely, for all $j \in [1, 4]$, a first draw picks up a value of a_j within JWST Gaussian distribution (rather than the specific central value $< a_j >$) and a second draw gives a_j^δ based on a standard deviation that can be different from that of JWST (σ_j). Figure 6 illustrates this strategy within a real case in which the error associated to each coefficient is 30% of the JWST data spatial distribution.

Figure 6: Determination of an a_j^δ set drawn from JWST correction coefficients a_j ; a_j^δ are randomly selected in a gaussian distribution centered on a_j with a dispersion which is a portion of σ_j (for instance here 30% of σ_j).
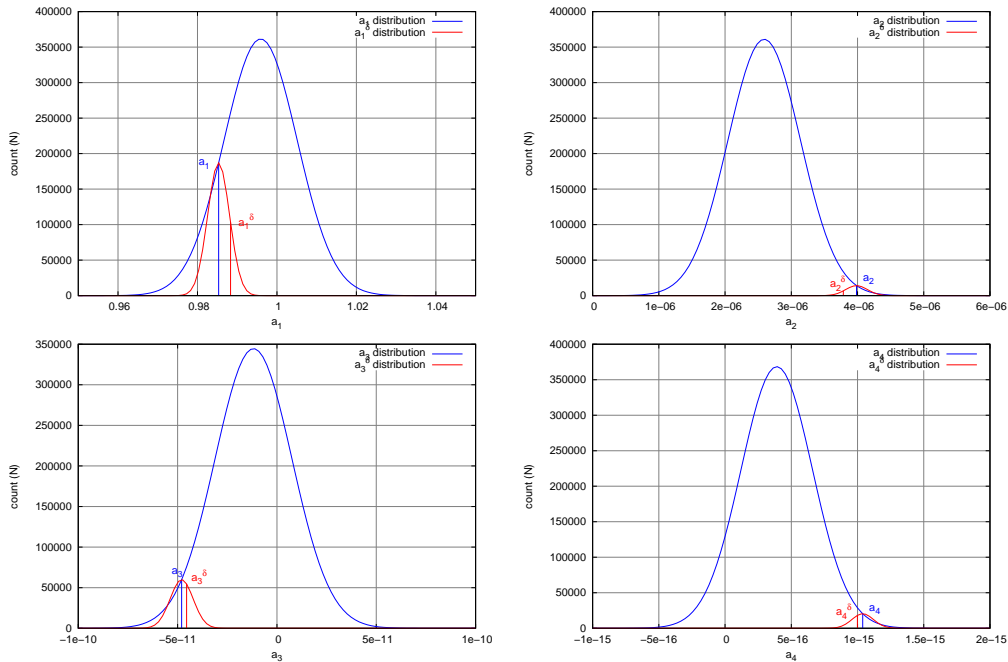
3.2 In-flight correction method

If the correction is applied on board, it is not possible to apply an individual correction to each pixel, because of warm-electronic limitations in term of storage capacity. That is why a common correction function is defined and applied to all pixels. This function also has a polynomial form of degree four and its coefficients can be calculated, for example, as the mean value of all individual coefficients $\overline{a_j^\delta}$.

Each read is then corrected by the non-linearity correction thus defined. The flux is finally measured using a linear fit of these data and relative correction error defined to be:

$$E = \left| \frac{f_{rec} - f_{exp}}{f_{exp}} \right|$$

where f_{rec} is the reconstructed flux, obtained after this operation and f_{exp} is the expected one.

3.3 On-ground correction method

If the correction is applied on-ground, an individual correction can be applied to each pixel but only on the straight line fit made in-flight and not to each read. The method is illustrated in figure 7. It consists in transforming the end-point of the straight line resulting from an exposure by the individual non-linearity correction of each pixel. The slope of the line passing through the transformed point is the reconstructed flux. Note that the proposed method has the merit of not being dependant on any zero fluctuation. For comparison with the in-flight correction, the relative correction error is also evaluated as defined above.

Figure 7: Non-linearity correction on-ground: 1. the non-linear signal is fitted in-flight by a linear function; 2. the linear function has the property of being able to be shifted to pass through the two extreme points of the adjusted signal (by property of polynomials); 3. non-linearity correction is applied to the twin points obtained, linear extrapolation is finally superimposed on expected signal.
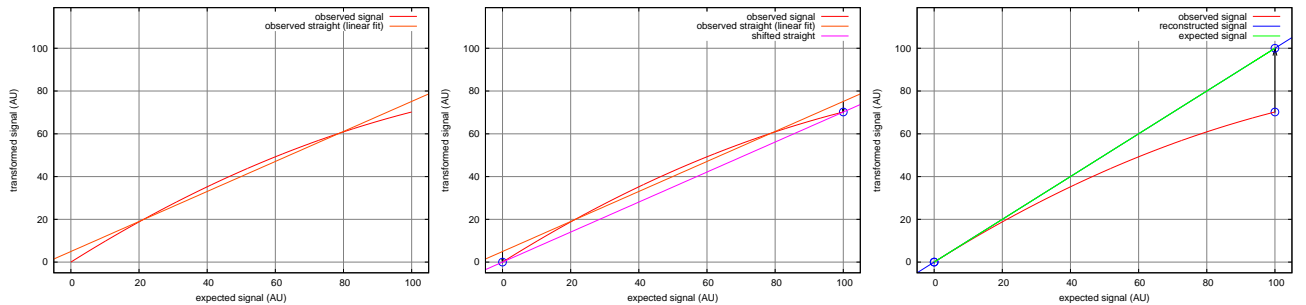
# 4 Systematic errors induced by each method of non-lineartity correction

In this section, non-linearity correction coefficients core supposed to be known precisely. This way, figures 8 and 9 illustrate only systematic errors induced by each method, using JWST data.

4.1 Impact of the readout mode

Figure 8 shows the impact of the readout mode on the non-linearity correction for both correction strategies: in-flight or on-ground. Flux is fixed to 2 e$^-$/pix/s and integration time is set to 565s.

Figure 8: Non-linearity correction effect versus readout mode for a flux of 2 e$^-$/pix/s
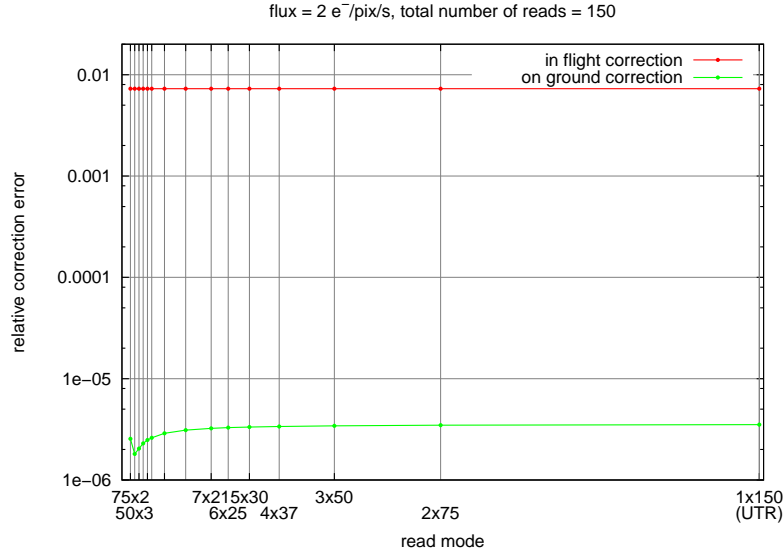
In-flight and on-ground methods do not strongly depend on the readout mode. The systematic error induced by non-linearity correction on-ground is about 2×10^{-6}, while it is about 7×10^{-3} in-flight.

We also checked that neither the number of reads per exposure nor the exposure time have a significant effect on systematic error induced by each method.

4.2 Impact of the integrated flux

As shown in figure 9, the systematic error induced by each method of non-linearity correction also depends on integrated flux. It is about 6.7×10^{-3} in-flight up to 30 e$^-$/pix/s ($\sim$17000 e$^-$/pix integrated signal) and increases then, exceeding 0.01 for fluxes higher than 75 e$^-$/pix/s ($\sim$42000 e$^-$/pix integrated signal). Applied on-ground, non-linearity correction induces a systematic error at least one order of magnitude lower, which also increases when the integrated flux increases.

Both non-linearity correction methods present systematic errors lower than 0.01 in the range in which Euclid will take data. Then, this study has to be extended to spectroscopic and photometric modes. That is the purpose of next section.
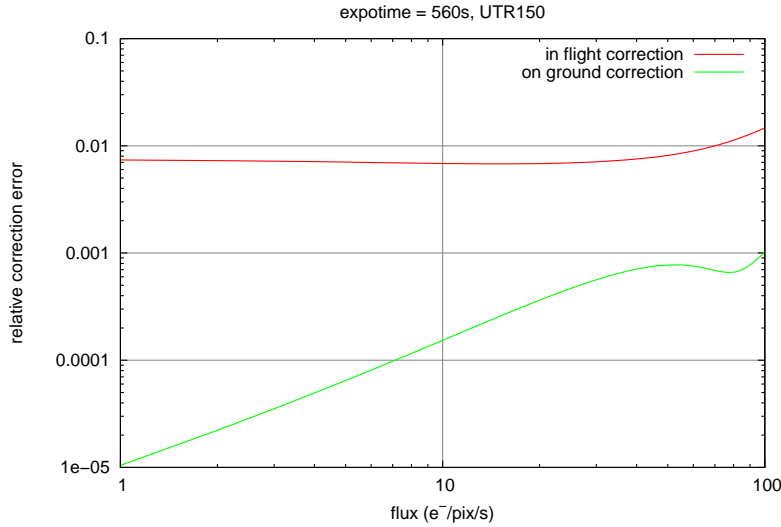
Figure 9: Non-linearity correction effect versus flux in UTR150 readout mode

5 Euclid science modes

5.1 Spectroscopic mode

In this section, we have a look at the impact of uncertainty on measurement of non-linearity correction coefficients with both methods. Let us remind that the required non-linearity correction must be performed to an accuracy of 1.5% for spectroscopy.

As the in-flight method uses mean values of the non-linearity correction coefficients, the error on them does not strongly change the error on the non-linearity correction, as shown in figure 10, although the dispersion of these errors is increased. The impact of the error on the non-linearity correction coefficients is higher for the on-ground method for which errors on the non-linearity correction coefficients should be lower than $0.8\ \sigma_{JWST}$ to be competitive with the in-flight correction method.

Figure 11 summarizes the impact of both methods for a flux varying from 0 to 3 e$^-$/pix/s and errors on the non-linearity correction coefficients up to $1.2\ \sigma_{JWST}$.

As shown in this figure, at low fluxes (< 3 e$^-$/pix/s), non-linearity correction error on-ground depends mainly on errors on the non-linearity correction coefficient. Non-linearity correction error can be lower than 4×10^{-3} if errors on the non-linearity correction coefficients do not exceed $0.3\ \sigma_{JWST}$. In-flight correction, on the contrary, is about 8×10^{-3} regardless of integrated flux or errors on the non-linearity correction coefficients.

5.2 Photometry mode

A similar simulation has been proceeded for photometric mode, for which the non-linearity correction requirements are quite harder to reach (0.3% accuracy).

Figure 10: Non-linearity correction effect versus uncertainty on the non-linearity correction coefficients for a flux of 2 e$^-$/pix/s
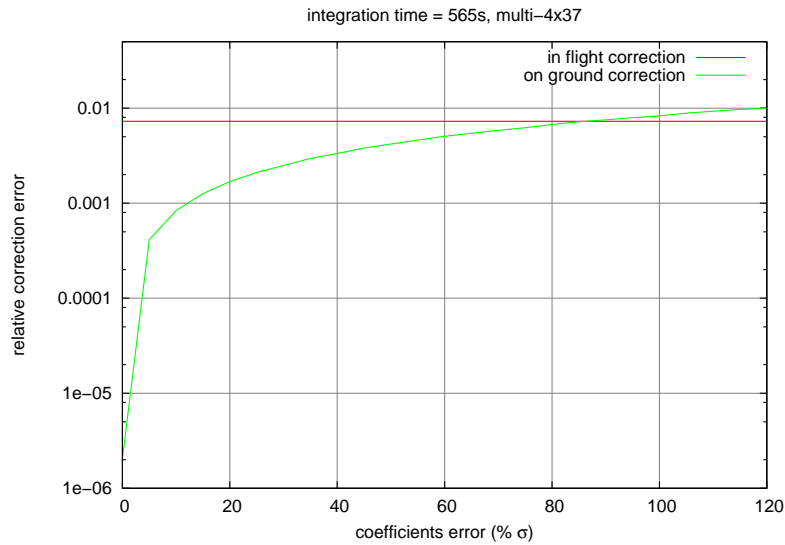

Figure 11: Non-linearity correction effect versus flux and uncertainty on the coefficients

Here, the in-flight method allows to reach $7{\times}10^{-3}$ as shown in figure 12, regardless of the dispersion of errors on the non-linearity correction coefficients.

Figure 12: Non-linearity correction effect versus uncertainty on the non-linearity correction coefficients for a flux of 2 e$^-$/pix/s

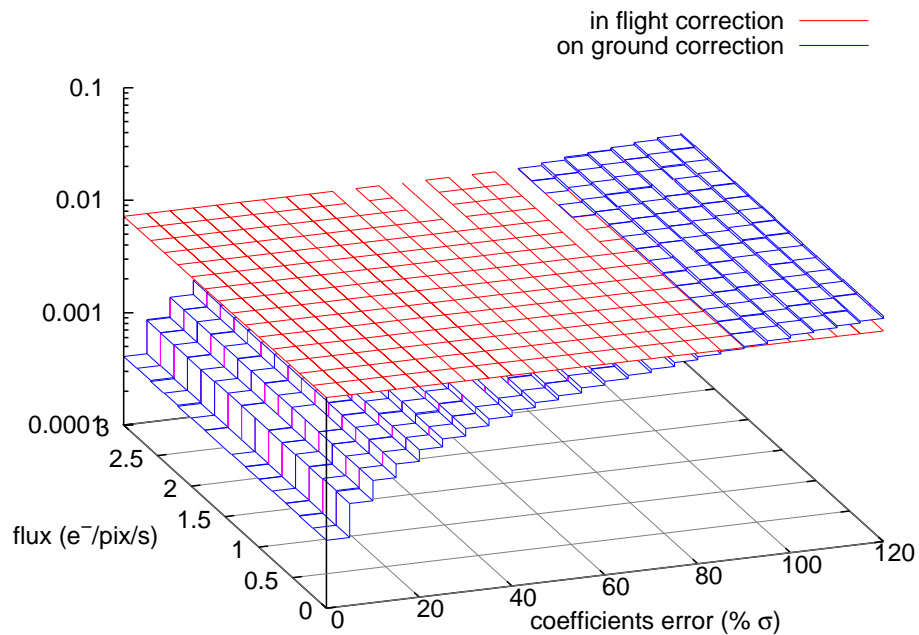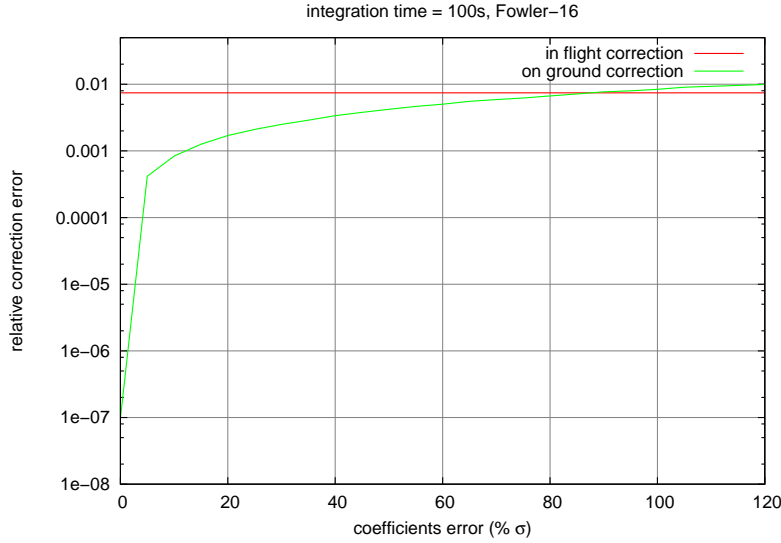Impact of the latter is stronger for the on-ground method for which the non-linearity correction accuracy is $3{\times}10^{-3}$ at 0.3 σ_{JWST} and exceeds $7{\times}10^{-3}$ at 0.9 σ_{JWST}. Thus, if error on the non-linearity correction coefficients is lower than 0.3 σ_{JWST}, a 0.3% accuracy on the non-linearity correction can be reached, at least at low fluxes ($<$ 3 e$^-$/pix/s).

This can also be seen in figure 13 which illustrates the fact that for low fluxes ($<$ 3 e$^-$/pix/s), non-linearity correction error does not strongly depend on the integrated flux but only on the errors on the non-linearity correction coefficients.

So, the in-flight method does not allow to reach an accuracy of 0.3% on non-linearity correction, for photometry mode, while the on-ground one does, provided that the non-linearity correction coefficients are measured with 0.3 σ_{JWST} accuracy.

6 Measurement of non-linearity correction coefficients

Simulation tools allow to determine the number of exposures needed to measure non-linearity correction coefficients with a sufficient accuracy to correct their effects on science mode with the required precision. In this section, we describe how we proceed to measure these non-linearity correction coefficients. It is not related to the dispersion in JWST data σ_{JWST} introduced above.

The method consists in simulating the non-linear response of a pixel at different fluxes. These fluxes are chosen so as to reconstruct properly the polynomial non-linearity response of the pixel for any flux within Euclid's data range, supposing that calibration exposures can be taken during the

Figure 13: Non-linearity correction effect versus flux and uncertainty on the coefficients
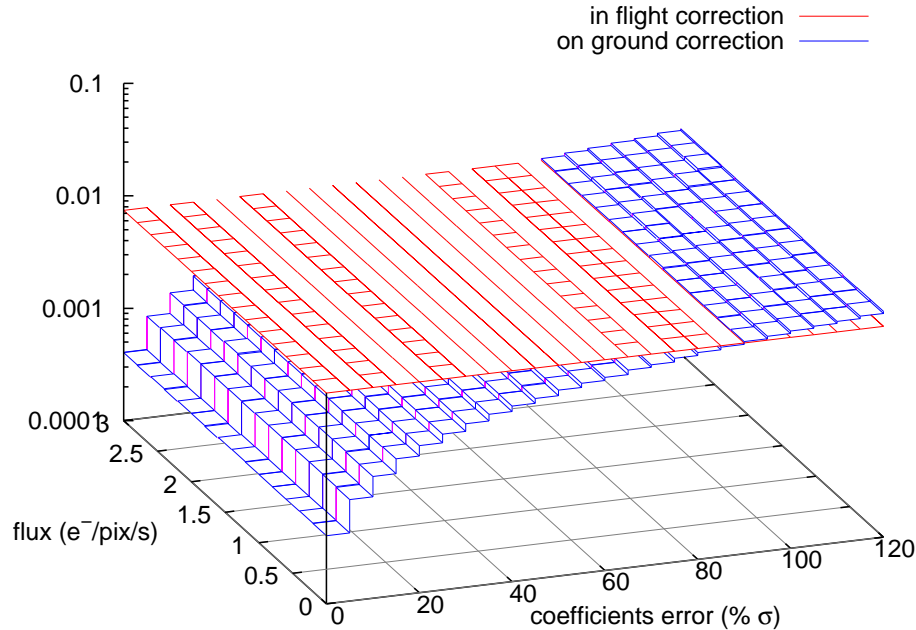
slewing time of the satellite (300s). Then, we apply the reconstructed non-linearity correction to the initial response of the pixel to science modes (spectroscopy and photometry) and compare it to the expected slope. Finally, the quality of non-linearity correction is defined as the relative difference between reconstructed slope and expected slope, which strongly depends on incident flux.

We assume in this document that warm-electronic enables to transfer at least 17 coadded frames per exposure, Poisson fluctuations during signal acquisition are taken into account and a CDS noise of 12 electrons is added.

Then the choice of calibration fluxes is not unique and here is a purpose in which calibration exposures are divided into cycles, each of them containing 20 consecutive calibration exposures. Their repartition is described in table 2. We tried to minimize the number of fluxes needed to measure non-linearity coefficients with required accuracy for any flux in the range of Euclid's data.

Figure 14 illustrates the fitting procedure, using 8 cycles as described in table 2. A larger concentration of measurements is needed at low fluxes because these are dominated by Poissonian fluctuations while polynomial coefficients are very sensitive to this region.

Figures 15 and 16 show the quality of non-linearity correction (for photometry and spectroscopy modes) versus the number of calibration exposures for various fluxes from 0.25 e$^-$/pix/s to 200 e$^-$/pix/s. The number of calibration exposures is a multiple of 20, corresponding to an integer of cycles as described in table 2.

As seen in these figures, non-linearity can be corrected on-ground with an accuracy better than 0.3% in photometry mode for fluxes higher than 2 e$^-$/pix/s. Achieving this precision requires about

Table 2: Used fluxes in a cycle of 20 calibration exposures

Fluxes (e$^-$/pix/s)	Maximum signal (e$^-$/pix)	Calibration exposures
0.5	150.	9
1.	300.	4
10.	3000.	6
190.	57000.	1
total		20

Figure 14: Determination of non-linearity calibration coefficients using a polynomial fit; left: on full scale; right: at low fluxes
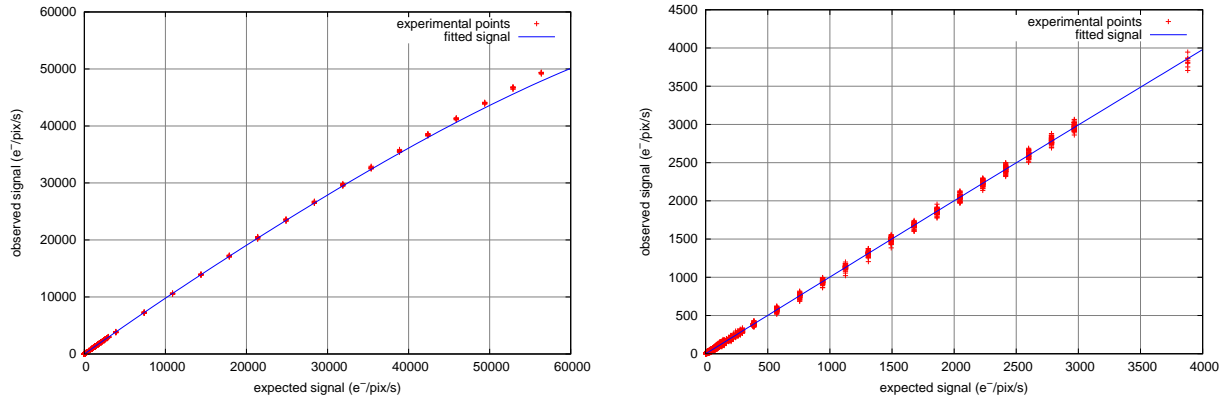

Figure 15: Quality of non-linearity correction versus number of calibration exposures in photometry mode; left: at low fluxes; right: at high fluxes
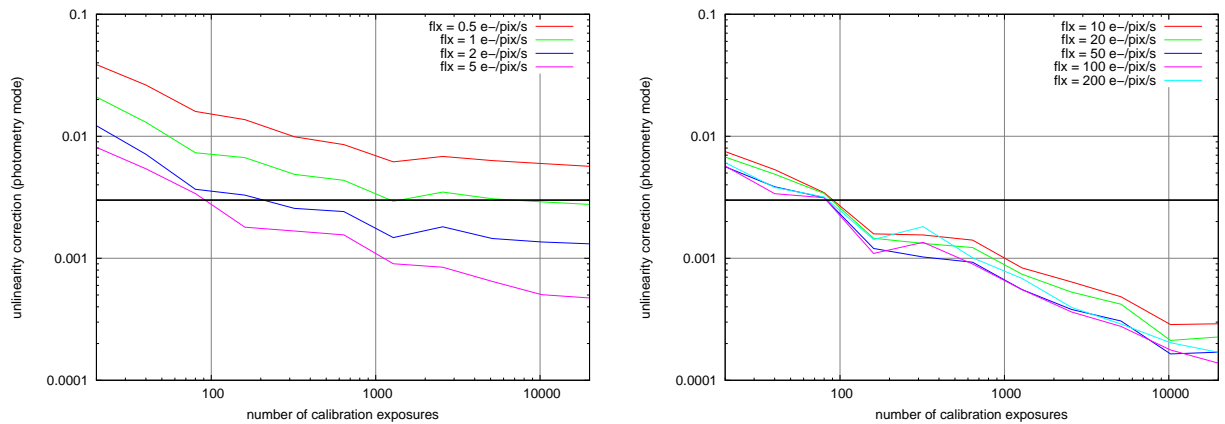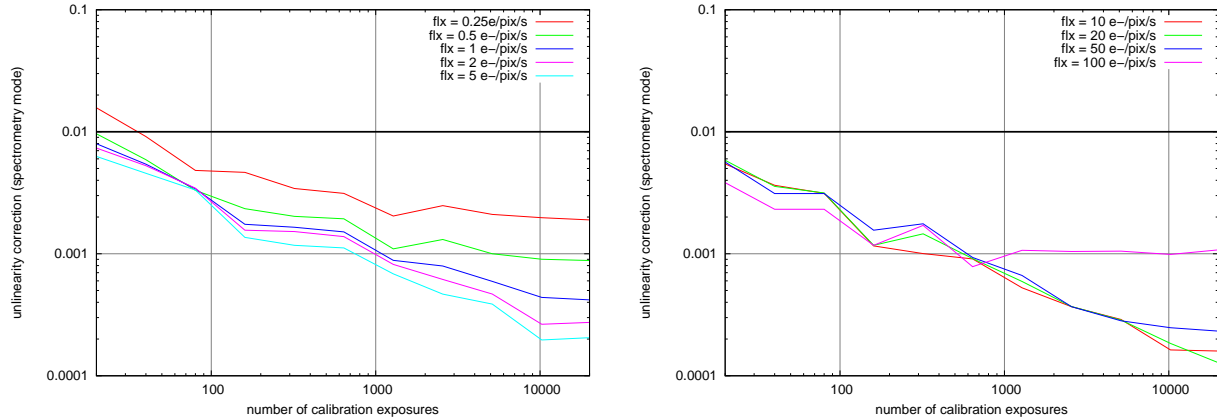
Figure 16: Quality of non-linearity correction versus number of calibration exposures in spectroscopy mode; left: at low fluxes; right: at high fluxes

200 exposures (10 cycles) with at least 4 light intensities and 17 coadded frames per exposure.

Using this method, all fluxes higher than 2 e$^-$/pix/s can be corrected with an accuracy better than 0.3% in photometry mode (and 0.5% for a flux of 1 e$^-$/pix/s). Moreover, regardless of the flux greater than 0.25 e$^-$/pix/s, the non-linearity correction is better than 1% in spectroscopy mode.

Once again, calibration procedure has been tuned to minimize the number of calibration fluxes to achieve the required accuracy for any flux in full range. If the number of calibration fluxes can be increased, it means that the number of calibration exposures can be reduced.

Note also that it is not a main issue to produce high fluxes with an instability negligible compared to Poissonian fluctuations of the signal, but it could be more difficult to build sources with very low fluxes. If it proves impossible to produce such sources with fluxes in the order of an electron, one solution is to implement a transparent mode in the warm-electronic to reduce the exposure time, and therefore the total integrated flux by an order of magnitude, especially because low fluxes are very important for a correct determination of non-linearity correction coefficients, as described above.

7 Key points

7.1 Reset anomaly

As shown in figure 1, the non-linearity effect increases when the integrated flux also increases. So, it is quite low at low fluxes as is the case of the Euclid mission (1 e$^-$/pix/s to 2 e$^-$/pix/s). However, the low flux area can suffer from a so-called *reset anomaly*.

Reset anomaly is characterized by non-linearity in the early frames following pixel reset. Although the reset anomaly appears to be unrelated to response linearity, these early frames nonetheless fall below a line projected through the later, asymptotic portion of the ramp.

One common solution to overcome its potentially detrimental side effects is to discard the first few frames of each integration. Clearly, this is an inefficient use of time.

The reset anomaly is discussed in [1], according to which it is *nearly noiseless for JWST SCAs that have been tested. The reset anomaly was barely noticeable in at least one outstanding prototype SCA, H2RG-015-5.0μm (which is substrate-removed).*

The JWST data studied in this note do not suffer from any noticeable reset anomaly, as shown in figure 17.

Figure 17: Non-linearity effect (JWST) in ADC count
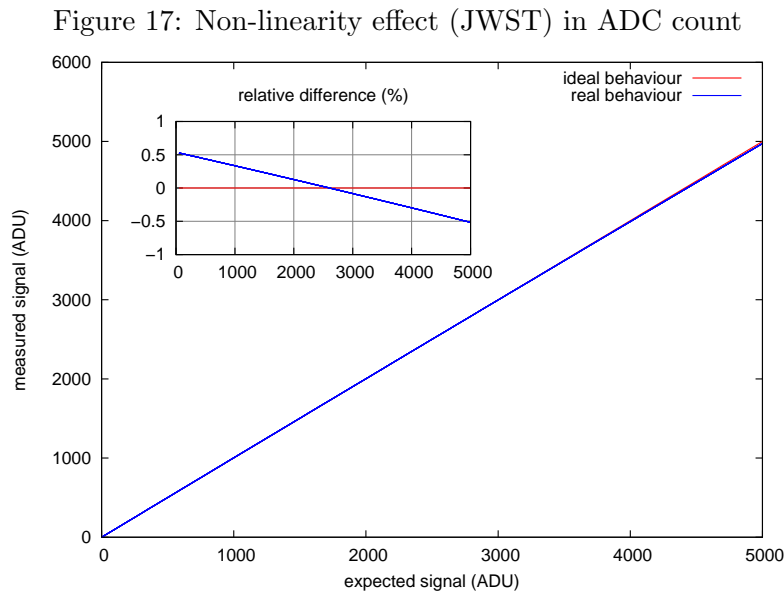
Although there are fears about the presence of a reset anomaly on Euclid detectors, nothing can be sure as long as we do not have our own measurements.

Moreover, the reset anomaly seems to be due to local (at the pixel cell level) temperature changes that occur when the clocking cadence is interrupted. When a pixel is read out, current flows through the pixel source follower FET and power is dissipated in the pixel. Slowing the readout cadence leads to cooling of the output FET and to a positive voltage change at the output. Increasing the readout cadence leads to local heating within the pixel, which appears as a negative signal at the pixel output. Continuously clocking and reading the detector may eliminate this effect.

We can expect to not observe any reset anomaly, but nothing portends that there will not be, and measurements are needed to answer this question.

---

[1]Detectors for the JWST Near-Infrared Spectrograph I: Readout Mode, Noise Model, and Calibration Considerations, Bernard J. Rauscher and Ori Fox

7.2 Reciprocity failure

So-called reciprocity failure characterizes the flux-dependent non-linearity that has already been observed in some near-infrared detectors [2]. It has to be distinguished from the standard non-linearity effect described in this note and can be measured by varying the flux for exposure times that produce a constant integrated signal.

Spatial non-uniformity of reciprocity failure across a detector will alter the apparent device uniformity as a function of the illumination intensity.

Note also that reciprocity failure may be "frozen out" at sufficiently low temperature.

7.3 Proposed test plan

If reset anomaly is due to temperature changes at the pixel cell level, it can be measured using different clocking cadence with interruption of it or not between exposures. This test can be performed using a flat field at low flux (to maximize the reset anomaly effect).

If a reset anomaly appears, we will have to study its form as a function of different parameters which can be linked to temperatures, time, fluxes, clocking cadence... Ideally, it should be described by an analytic form and substracted to each exposure. Obviously, this implies studying influence of each parameter on reset anomaly...

Reciprocity failure also needs to be measured using real data. It consists in a set of three exposures, each using different flat field illuminations during a time such as integrated signal should be the same at the end of each exposure. This set of measurements should be repeated a few times at different temperatures to test the effect of this latter on the reciprocity failure.

Reciprocity failure is all the more important than it could affect the non-linearity monitoring which can be performed in-flight during Euclid mission if low integrated fluxes obtained by adjusting exposure time.

8 Conclusion

This document demonstrates the feasibility of the two correction methods described here: in-flight and on-ground.

According to JWST data, we found that using at least 4 light intensities and at least 17 coadded frames per exposure, non-linearity can be corrected on-ground with an accuracy better than 0.3% on photometry mode for fluxes higher than 2 e$^-$/pix/s and better than 1% on spectroscopy mode, regardless of the flux provided greater than 0.25 e$^-$/pix/s. In-flight corection, on the other hand, does not enable to reach an accuracy better than 7×10^{-3} on photometry mode, regardless of the flux, but has the advantage to not be sensitive to a single pixel non-linearity correction deviation (which is otherwise expected very low).

---

[2]Final Performance Report "Precision Photometry to Study the Nature of Dark Energy", W. Lorenzon and M. Schubnell

Regarding these results, we suggest to apply non-linearity corection on-ground and control in-flight any non-linearity drift of pixels by the method described in section 6. This control can be performed each six months, during slewing time of the satellite.

Remains to verify the possibility of producing light sources delivering the required fluxes with sufficient stability during the time required for calibration. Question arises especially at low fluxes because of the difficulty to obtain an illumination of 0.5 e^-/pix/s. This key point can be solved using a light source ten times more intense if warm-electronic enables to use a transparent mode with consecutive single frames to reduce the exposure time. This way, integrated flux can be the same in ten times less exposure time. This also has the effect of reducing the calibration time of non-linearity correction coefficients.

Note also that this study is based on the analysis of JWST data on a detector that did not present any noticeable reset anomaly, but we can not conclude with certainty that it will be the case of the Euclid ones.